

A Priori Study of Models for Large Eddy Simulations of Drop-Laden Flows

Nora A. Okong'o and Josette Bellan*

Jet Propulsion Laboratory, California Institute of Technology, Pasadena, CA 91109-8099

Abstract

Large Eddy Simulation (LES) models are evaluated on a Direct Numerical Simulation (DNS) database representing a three-dimensional temporal mixing layer with evaporating drops. In two-phase flow LES, necessary models must be found for the filtered source terms representing the effect of the drops on the filtered flow field. Because the unfiltered flow field, unavailable in LES, is required for calculating the source terms, various approximations were considered for it, and a reduction in the number of tracked drops was evaluated. All filtered source term models were found to overestimate corresponding filtered source terms, and the error of using computational drops was calculated.

Introduction

The Large Eddy Simulation (LES) methodology was conceived for single-phase (SP) flows to decrease computational costs through restricting the resolution to that of the large scales and including the effect of the small scales through models. The LES equations are obtained by spatially filtering the Direct Numerical Simulation (DNS) equation set, as DNS are simulations which compute the entire range of scales typical of turbulent flows. For compressible multi-species flows, this filtering process introduces unresolved momentum, energy and species subgrid scale (SGS) fluxes. Therefore, for SP flows, the necessary SGS models consist of expressions relating the SGS fluxes to the resolved variables. For two-phase (TP) flows with evaporating (liquid) drops, the situation is more complicated because the filter volume contains drops. Assuming that the drops are small enough to be treated as point sources, their evolution depends on the gas-phase flow field, and in turn they affect the gas phase by acting as sources of mass, momentum and energy. Consistency in the goal of decreasing computational costs dictates that not only must the flow resolution be decreased in LES with respect to DNS, but the same concept also must be applied to the ensemble of drops. That is, in LES the drops should not be the actual drops of DNS, but instead should be 'computational' drops representing the effect of several actual drops. Therefore, TP LES requires modeling both the effect of the flow field on the drops (through the drop far-field), and that of the drops on the flow field (through filtered source terms).

We use here the DNS database from a recent study [1] to

develop the necessary models for the filtered source terms (SGS flux models are derived elsewhere [2]) with the intent of introducing a consistent TP flow LES methodology wherein both the number of grid points and that of tracked drops is reduced compared to DNS. SGS TP flow models that treated the drop contribution but did not reduce the size of the drop ensemble or consider the effect of the drops on the flow field were presented in [3] and [4]. Some of these models are here extended so as to calculate the filtered source terms from the filtered flow field and the reduced drop ensemble. Only an abbreviated description of the source term modeling study is here presented, with details available elsewhere [2].

Highlights of the DNS model

The detailed DNS equations along with the justification of the assumptions embodied in them were described in [1], based on the formulation of [5]. The governing equations are formulated in an Eulerian frame for the gas phase and a Lagrangian frame for the drops. The gas phase consists of two species which are the carrier gas and the vapor evolving from the drops. In contrast with the formulation of [5], the gas energy equation of [1] includes the heat flux contribution due to the enthalpy carried by the species. The drops are treated as point sources of mass, momentum and energy for the gas phase; this treatment is justified by the dilute (i.e. volumetrically small, $O(10^{-3})$) loading and the size of each particle being much smaller than the Kolmogorov scale.

The mixing layer geometry is illustrated in Fig. 1 where the streamwise (x_1), the cross-stream (x_2), and the span-

*Corresponding author: josette.bellan@jpl.nasa.gov. Proceedings of the Third Joint Meeting of the U.S. Sections of The Combustion Institute

wise (x_3), coordinates are shown, and the domain lengths are L_1 , L_2 and L_3 in each direction. Periodic boundary conditions are used in the x_1 and x_3 directions, and adiabatic slip wall conditions are employed for the x_2 boundaries. The free-stream velocity $U_0 = M_{c,0}a_{c,0}$ is calculated from a specified value of the convective Mach number $M_{c,0}$ based on the carrier gas initial speed of sound $a_{c,0} = \sqrt{R_C T_{C,0} C_{p,C} / C_{v,C}}$ where $T_{C,0}$ is the initial uniform temperature of the carrier gas at the initial uniform pressure; the carrier gas is the sole initial species in the gas phase. The initial vorticity thickness is $\delta_{\omega,0} = \delta_{\omega}(0)$ where $\delta_{\omega}(t) = \Delta U_0 / (\partial \langle u_1 \rangle / \partial x_2)_{\max}$ with the brackets $\langle \rangle$ denoting averages over homogeneous (x_1, x_3) planes and the velocity difference across the layer is $\Delta U_0 = 2U_0$; the initial mean streamwise velocity has an error-function profile. The specified value of the initial Reynolds number, $Re_0 = \rho_0 \Delta U_0 \delta_{\omega,0} / \mu$, where ρ_0 is the initial gas density, is used to calculate μ . The thermal conductivity and diffusivity are then computed using this value of μ and specified values of Prandtl and Schmidt numbers of 0.697 (the Lewis number is unity). All thermophysical properties are the same as those employed in the simulations of [3] using air as the carrier gas and decane as the drop liquid.

To promote layer growth, the layer is initially perturbed so as to induce roll-up and pairing. The perturbations, described in [5] specify spanwise and streamwise vorticity fluctuations, with streamwise and spanwise wavelengths in the x_1 and x_3 directions of $\lambda_1 = 7.29\delta_{\omega,0}$ and $\lambda_3 = 0.6\lambda_1$. For all the simulations performed herein, $L_1 = 0.2$ m, $L_1 = 4\lambda_1$, $L_2 = 1.1L_1$ and $L_3 = 4\lambda_3$, where L_i is the domain length in the x_i direction. The relative amplitudes of the forcing perturbations with respect to the circulations are 10% and 2.25% in the spanwise and streamwise directions, respectively.

The drops are initially distributed randomly throughout the $x_2 < 0$ domain with specified temperature, velocity, number density and size distribution. Initially, all the drops have the same temperature, $T_{d,0}$, and have the same velocity as the gas phase at their location. The mean number density profile is smoothed near the center-line, $x_2 = 0$, using an error function profile. The drop size distribution is initially specified through the drop Stokes number $St = \tau_d \Delta U_0 / \delta_{\omega,0}$ whose initial distribution is Gaussian with mean 3 and standard deviation 0.5. The number of drops is determined by the initial mass loading ML_0 (initial ratio of mass of liquid to mass of carrier gas in drop-laden part of domain).

The DNS equations were solved numerically using a fourth-order explicit Runge-Kutta temporal integration for time derivatives and eight-order central finite differences with tenth-order filtering for spatial derivatives. A fourth-

order Lagrange interpolation procedure was used to obtain gas-phase variable values at the drop locations. The DNS endeavor was undertaken to achieve several transitional states that could be further analyzed for *a priori* turbulence modeling. As detailed in [1], simulations were performed at $Re_0 = 500$ and 600 and at ML_0 of 0, 0.2 and 0.5. All cases had $M_{c,0}=0.35$, $T_{C,0}=375K$, $\rho_0=0.9415kg/m^3$, $\Delta U_0=271.7m/s$ and $\delta_{\omega,0}=6.859 \times 10^{-3}m$. The drop laden ($ML_0 > 0$) cases had $T_{d,0}=345K$ and liquid density of $642kg/m^3$. In the present paper, the *a priori* source-term analysis is restricted to the simulation with $Re_0 = 600$ and $ML_0 = 0.2$, denoted TP600a2, which had 2,993,360 drops, $288 \times 320 \times 176$ grid points; at the transitional state which occurred at the nondimensional time ($t^* = t\Delta U_0 / \delta_{\omega,0}$) of 105, this layer attained a momentum-thickness Reynolds number of 1576.

Models for filtered source terms

There are two issues in modeling the drops source terms in LES: (i) the necessity of knowing the gas flow dependent variables at the drop locations, and (ii) the consistent reduction, in the spirit of LES, of the number of tracked drops to match the reduction in the number of computational nodes from DNS to LES. The first issue has initially been studied in [4] and further in [1]. Several models were evaluated by comparison with the DNS database: (1) an ideal model which precisely replicates the flow field (unattainable in LES and representing the best-case scenario in which errors due to modeling the unfiltered flow field are eliminated), (2) a baseline model which neglected SGS effects on the drop evolution, (3) a random model with a mean specified by the LES solution and a SGS standard deviation, σ_{SGS} , to be modeled, and (4) a deterministic model which reconstructs the DNS field at the drop location based on a Taylor expansion resulting in a model (subscript m)

$$\psi_m = \tilde{\psi} - \bar{\sigma} \text{sign}(\nabla^2 \tilde{\psi}), \quad (1)$$

with the filtered standard deviation $\bar{\sigma} = \sqrt{\bar{\sigma}^2}$ modeled as

$$\bar{\sigma}^2 = \left(\sqrt{\overline{\psi\psi}} - \sqrt{\overline{\tilde{\psi}\tilde{\psi}}} \right)^2 = \left(\sqrt{\sigma_{SGS}^2 + \overline{\tilde{\psi}\tilde{\psi}}} - \sqrt{\overline{\tilde{\psi}\tilde{\psi}}} \right)^2, \quad (2)$$

where $\psi(\phi) = \{u_i, T, Y_V, p\}$ represents the gas-phase primitive variables (u_i is the i th component of the velocity, T is the temperature, Y_V is the evaporated vapor mass fraction and p is the pressure) and $\phi = \{\rho, \rho u_i, \rho e_t, \rho Y_V\}$ represents the gas-phase conservative variables (ρ is the density and e_t is the total energy). By definition, $\tilde{\psi}$ is the volume-average associated with a filter G and $\psi = \overline{\rho\psi} / \bar{\rho}$ is the Favre (density-weighted) filtering. Using the best available σ_{SGS} , as calculated from

the DNS database in order to decouple the assessment of the reconstruction process from the issue of modeling $\tilde{\psi}$ and σ_{SGS} , it was shown [2] that the DNS source terms $S_d(\psi_f, Z) = \{S_{I,d}, S_{II,i,d}, S_{III,d}\}$ at the drop locations and filtered source term $\bar{S}(\psi_f, Z) = \frac{1}{V_f} \sum_{\beta} [S_d(\psi_f, Z)]_{\beta}$ source terms calculated on the actual drop field Z are best reproduced by the model eqs. 1 and 2; the ideal model used in conjunction with Z leads to the DNS fields, but is not attainable in LES. ψ_f is the value of ψ at the drop far-field, $S_{I,d}, S_{II,i,d}$ and $S_{III,d}$ are the source terms in the continuity, momentum and energy equations, $\bar{S} = \{\bar{S}_I, \bar{S}_{II,i}, \bar{S}_{III}\}$ is the filtered source term and V_f is the filtering volume where there are β drops.

To study the issue of reducing the number of computed drops, we consider that each computational drop represents a fixed number of actual drops. That is, if the number of real drops is N_{α} and the number of computational drops is N_{β} , then each computational drop β represents N_R drops, where $N_R = N_{\alpha}/N_{\beta}$ is the ratio between the number of actual drops and the number of computational drops. The filtered source terms are then computed for the N_{β} drops, and scaled by N_R leading to

$$\bar{S}_m(\psi_{f,m}(\bar{\phi}), \bar{Z}) = N_R \sum_{\beta} \frac{1}{V_f} [S_d(\psi_{f,m}(\bar{\phi}), \bar{Z}(N_R))]_{\beta} \quad (3)$$

where \bar{Z} is a representative drop field rather than the actual drop field Z . To illustrate the effect of increasing N_R (decreasing the number of computational drops), in Fig. 2 are the (x_1, x_3) homogeneous-plane averages and RMS of \bar{S}_I and its models. A top-hat filter is used with width $\bar{\Delta} = 4\Delta x$ or $\bar{\Delta} = 8\Delta x$, where $\Delta x = \max(\Delta x_1, \Delta x_2, \Delta x_3)$ is the grid spacing with $\Delta x_1 \simeq \Delta x_2 \simeq \Delta x_3$ for the DNS. The results for \bar{S}_m are labeled according to the ψ_m used (ideal, baseline, random, deterministic), while those for \bar{S} are labeled as ‘exact’. These plots for $N_R = 1, 8$ and 64 are not intended to be typical, but rather to visualize the global comparisons to be presented below. Clearly, in the middle of the layer there is strong evaporation, as indicated by the average \bar{S}_I being positive. In the lower stream, on average \bar{S}_I is negative, indicating net condensation; further scrutiny revealed that at some locations there is also evaporation occurring. As shown by the small RMS in the lower stream, the magnitude of condensation/evaporation is small. Returning to the issue of computational-drop modeling, Fig. 2 shows that \bar{S}_I is generally overpredicted by the models. Whereas on average, the models do not seem to show much dependence on N_R , the RMS shows a clear deterioration with N_R . The greatest error in $\bar{S}_{I,m}$ occurs in the middle of the layer where the strongest evaporation occurs and where the filtered flow field differs most from the unfiltered flow field. In contrast, near the boundaries the filtered flow field

is almost identical to the unfiltered one. Since the models are relatively more accurate at the lower stream boundary, where the non-zero \bar{S}_I shows that the drops are still evaporating/condensing, the indications are that drop evaporation is not by itself the cause of errors in the filtered source term models. Rather, errors arise from the imprecision in representing the actual drop field by the computational drop field, since the ideal model (which uses the actual unfiltered variables) gives the same results as the other models near the lower boundary. Given that the errors due to modeling the unfiltered flow field are unavoidable in LES, it is of interest to determine the conditions under which the additional errors introduced by the computational-drop modeling are acceptably small.

To quantify the effect of increasing N_R , slopes from the least square fits of the filtered DNS (i.e. \bar{S} computed at the corresponding $\bar{\Delta}$) to modeled $\bar{S}_I, \bar{S}_{II,i}$ and \bar{S}_{III} are plotted (see [2]) for $\bar{\Delta}$ of $4\Delta x$ and $8\Delta x$ versus $N_R = 1, 2, 4, 8, 16, 32, 64$. The results show that all slopes are smaller than unity, meaning that all the models overestimate the source terms. Generally, the deterministic model outperforms the baseline model, with errors almost halfway between those of the baseline and ideal models, and the random model is the worst. Consistently, the ideal model gives the best prediction for \bar{S} ; its relative superiority is significant at the larger filter width, and at the smaller filter width when N_R is small. For the smaller filter width at larger N_R , all the models give similar predictions. The accuracy of the models declines with N_R , but not at the same rate for all source terms as \bar{S}_{III} seems to be best predicted whereas $\bar{S}_{II,3}$ seems to be the worst predicted with the strongest error growth with N_R . It can thus be concluded that for small N_R (more computational drops) the inaccuracies in $\psi_{f,m}$ are a much stronger source of error than is the effect of computational-drop modeling ($N_R > 1$). This explains why, when using ψ_f , it is seen that the ideal model \bar{S}_m improves for fixed N_R as $\bar{\Delta}$ is increased from $4\Delta x$ to $8\Delta x$ since the filtering volume is increased and the number of drops within each filtering volume is accordingly increased, giving a better accuracy; whereas the opposite is observed with all the other \bar{S}_m because as $\bar{\Delta}$ increases, information is lost during the gas-phase variable modeling, resulting in decreasing accuracy (as $\bar{\Delta}$ increases, $\tilde{\psi}$ is more unlike ψ). However, for large N_R (fewer computational drops), larger than about 8, the effect of having few drops dominates, as there is an increasing convergence of the slopes from the ideal \bar{S}_m to those from the other \bar{S}_m for larger N_R . Also noticeable is the effect of the nonlinear relationship between $\psi_{f,m}$ and \bar{S}_m in that a proportional reduction in grid resolution and number of drops does not give the same error in the filtered source

terms. That is, increasing $\bar{\Delta}$ from $4\Delta x$ to $8\Delta x$ means an eight-fold increase in the filtering volume, but an eight-fold decrease in the number of drops ($N_R = 1, 2, 4, 8$ compared to $N_R = 8, 16, 32, 64$, respectively) does not give the same error in \bar{S}_m . In quantifying the \bar{S}_m error through the maximal percentage error (greatest deviation from unity over the five source terms, multiplied by 100), the maximal \bar{S}_m error was found to be in $\bar{S}_{II,3}$ for the baseline, random and deterministic models. The maximal percentage errors listed in Table 1 show that for the baseline model, the error for $N_R = 8$ and $\bar{\Delta} = 8\Delta x$ is three times that for $N_R = 1$ and $\bar{\Delta} = 4\Delta x$, whereas the error for $N_R = 64$ and $\bar{\Delta} = 8\Delta x$ is twice that for $N_R = 8$ and $\bar{\Delta} = 4\Delta x$. A similar trend of decreasing error ratio with increasing N_R is observed for the other models. When proportionally increasing N_R and the filter volume, the largest loss of accuracy is experienced with the deterministic model, which is the most accurate, while the smallest relative error is with the random model, which is the least accurate. In LES the effect of modeling ψ_f is unavoidable and most likely $\bar{\Delta}$ would have been selected according to the gas-phase resolution requirements; once $\bar{\Delta}$ is selected, the accuracy of the calculation will decrease with increasing N_R , independent of the model. This means that if large errors are computationally acceptable (i.e. order of magnitude calculations), a large N_R and large $\bar{\Delta}$ are acceptable because the error will be the same as for large N_R and small $\bar{\Delta}$; that is, for large N_R the error is independent of $\bar{\Delta}$.

The above results concerning the computational drops were obtained at a transitional state. It is pertinent to inquire whether the overprediction of the filtered source terms is unique to this time station, or rather a general occurrence. To this end, the analysis of \bar{S}_m was repeated at $t^* = 20, 45$ and 80 , corresponding to time stations before the first pairing, between the first and second pairings and at the end of the second pairing. The results reinforce the previous conclusions that: (1) the effect of modeling ψ_f is dominant at the larger $\bar{\Delta}$, where the error is initially large but not so sensitive to N_R , (2) the effect of modeling ψ_f is significant at the smaller $\bar{\Delta}$ for smaller N_R but not at larger N_R , (3) the deterministic model performs best, followed closely by the baseline model, with the random model giving the worst predictions, and (4) decreasing the number of computational drops proportionally to the increase in filtering volume size does not necessarily maintain the filtering error. In considering the pre-transitional time stations, the trends at a given N_R seem to be as follows: (1) for the smaller $\bar{\Delta}$, the error seems insensitive to time up to $t^* = 80$ and then exhibits a small growth, except for the lowest $N_R = 1$ or 2 where the error clearly grows with time, and (2) for the larger $\bar{\Delta}$, the error generally grows with time, with more pronounced error growth at smaller

values of N_R .

Conclusions

From this *a priori* study, the indications are that the unfiltered flow field models perform better for smaller filter widths; however, only at small values of N_R (below about 8 for $\bar{\Delta} = 4\Delta x$) does this translate into improved accuracy of filtered source term models. On the other hand, for larger filter widths, there is little to be gained by using small N_R , since the error growth with N_R is modest; however, the filtered source term models will be less accurate than at the smaller filter width. None of the models considered yields particularly accurate predictions for the filtered source terms, with errors ranging from 10% to 90%. However, this does not necessarily preclude their use in LES, since from the budgets of the LES equations ([1]), the filtered source terms are an order of magnitude smaller than the largest terms. The sensitivity of flow field and drop evolution to filtered source term errors can only be determined by performing an *a posteriori* LES study.

Acknowledgements

This work was conducted at the Jet Propulsion Laboratory of the California Institute of Technology under the sponsorship of the U.S. Department of Energy (DOE), with Mr. Neil Rossmeissl (DOE Headquarters) and Mr. D. Hooker (DOE Golden Center) serving as contract monitors, under an agreement with the National Aeronautics and Space Administration. Computations were performed on the SGI Origin 2000 at the JPL Supercomputing Center.

References

- [1] Okong'o, N., and Bellan, J., Consistent large eddy simulation of a temporal mixing layer laden with evaporating drops. Part I: Direct numerical simulation and formulation submitted to *Journal of Fluid Mechanics* (2002).
- [2] Okong'o, N. and Bellan, J., Consistent large eddy simulation of a temporal mixing layer laden with evaporating drops. Part II: *A priori* modeling, submitted to *Journal of Fluid Mechanics* (2002).
- [3] Miller, R. S., and Bellan, J., *Physics of Fluids* 12(3):650–671 (2000).
- [4] Okong'o, N., and Bellan, J., *Physics of Fluids* 12(6):1573–1591 (2000).
- [5] Miller, R. S., and Bellan, J., *Journal of Fluid Mechanics* 384:293–338 (1999).

	N_R	Baseline	Random	Deterministic
$E_{\max}(\bar{\Delta}, N_R)$	1	19	26	10
	2	22	32	13
	4	27	42	19
	8	36	54	30
$E_{\max}(2\bar{\Delta}, 8N_R)$	1	56	65	40
	2	60	72	45
	4	65	79	53
	8	73	87	64
$\frac{E_{\max}(2\bar{\Delta}, 8N_R)}{E_{\max}(\bar{\Delta}, N_R)}$	1	3.0	2.5	4.0
	2	2.8	2.3	3.5
	4	2.4	1.9	2.8
	8	2.1	1.6	2.1

Table 1: Maximal percentage error of filtered source term models, E_{\max} , for TP600a2 at $t^*=105$, $\bar{\Delta} = 4\Delta x$.

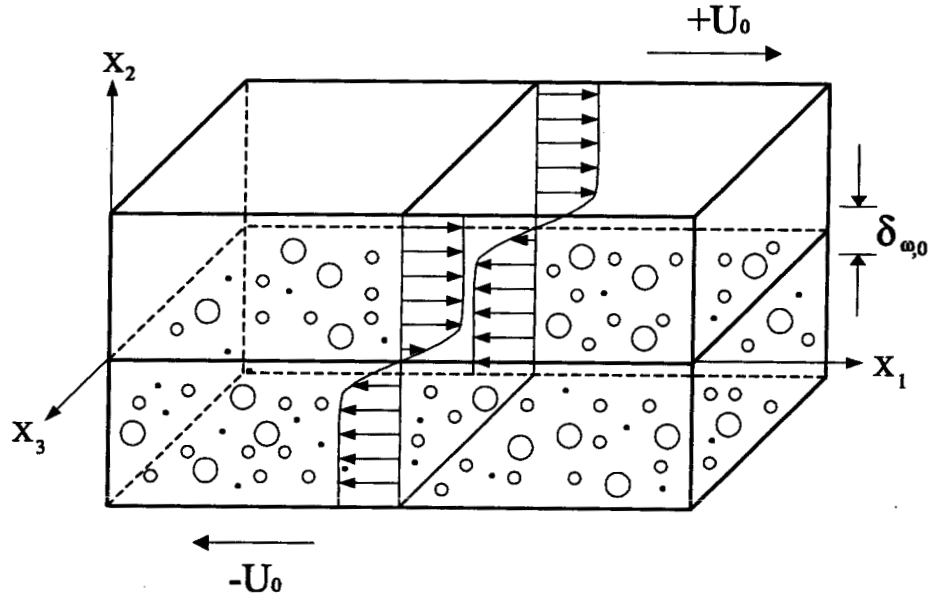


Figure 1: Mixing layer configuration

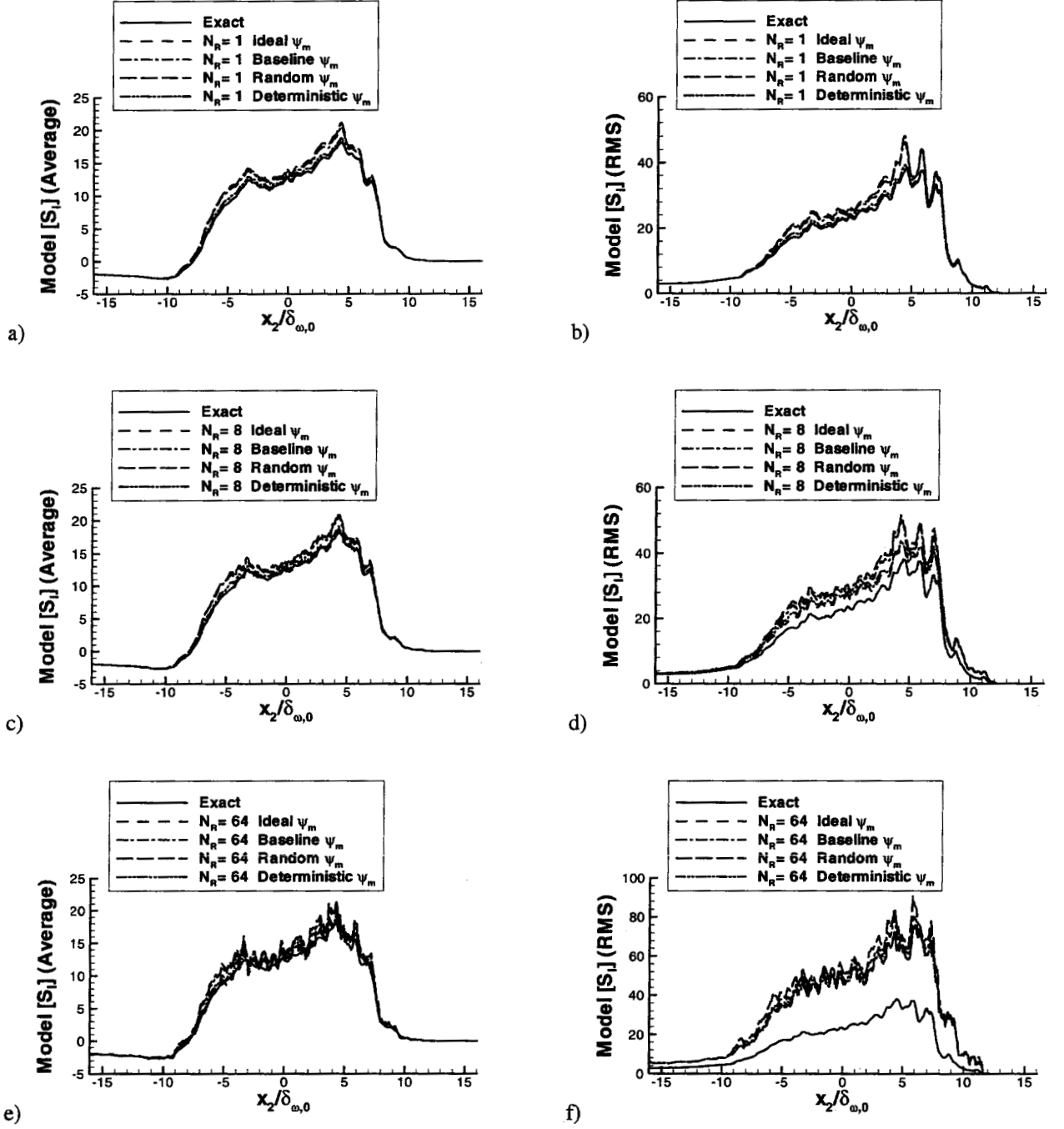


Figure 2: Homogeneous (x_1, x_3) plane (a,c,e) averages and (b,d,f) RMS of \bar{S}_I models, TP600a2 ($Re_0=600$, $ML_0=0.2$) at $t^*=105$, $\bar{\Delta}=4\Delta x$: (a,b) $N_R=1$, (c,d) $N_R=8$, (e,f) $N_R=64$. The filtered source term models are designated ideal, baseline, random or deterministic according to ψ_m , the model used for the unfiltered gas-phase variables. N_R is the ratio of the number of actual drops to the number of computational drops. (In the figures, the notations $[S]$ and Δ are used for \bar{S} and $\bar{\Delta}$ respectively.)